Indian Journal of Chemical Technology
Vol. 31, May 2024, pp. 394-410
DOI: 10.56042/ijct.v31i3.6451

Non-uniform energy source / sink influence on magneto-convective $CdTe$ and C/H_2O suspended Williamson fluid model: Computational approach

B. Vinothkumar & T. Poornima*

Department of Mathematics, School of Advanced Sciences, Vellore Institute of Technology, Vellore-632 014, Tamil Nadu, India

*E-mail: poornima.t@vit.ac.in

Received 29 October 2023; accepted 3 April 2024

The recent advances in nanotechnology have enabled the creation of hybrid-class nanofluids with superior thermal properties when compared to normal nanofluids. The dominant characteristics of hybrid nanofluids, such as rapid heat transfer rates, superior electrical and thermal conductivity, and cheap cost, have effectively piqued the interest of worldwide researchers. The current study examines the effects of energy transfer dynamics on a non-Newtonian fluid model suspended hybrid nanoparticles consisting of cadmium telluride ($CdTe$) and graphite (C) particles with water as base fluid under magnetic effects. The rheological impact and base fluid characterisation are determined using the Williamson fluid model. The impact of various flow affecting parameters on the momentum, temperature along with wall drag force and heat transfer rate is computed and studied in detail with the streamline portray. It is possible to compare the numerical results using the Keller box (finite differences) method with the help of MATLAB programming. The hybrid nanofluid cadmium telluride and graphite ($CdTe + C/H_2O$) has superior thermal conductivity than the nanofluids($CdTe$ *or* C), according to the data, which are presented in graph form. The numerical solutions for Nusselt number, velocity profile, skin friction coefficient, temperature profiles have been represented with the help of graphs.

Keywords: Hybrid nanofluid, Keller–Box numerical method, Magnetic Field, Non-uniform heat source and sink, Williamson fluid model

Introduction

The advent of the 21st century advocated the development of a new, more efficient thermal energy source to address the energy crisis. Energy has a crucial and fundamental function in heavy industries and technical processes. Applications for the movement of boundary layers and heat transfer include the drawing of polymer sheets, the extrusion of metals from dies, and the cooling of metallic plates in showers, among other things. Due to their excellent heat transfer abilities and ease of access, fluids are widely used for cooling applications.

In the realm of fluid dynamics and heat transfer, the quest for efficient and innovative solutions continually drives scientific exploration. Among the forefront areas of investigation lie Williamson fluid models, an intriguing class of fluid suspensions infused with nanoparticles known for their remarkable thermal conductivity enhancements. Concurrently, the discipline of Magnetohydrodynamics (MHD) commands attention for its ability to elucidate the complex interactions between magnetic fields and fluid flow, offering insights into phenomena ranging from astrophysical processes to industrial applications. Nanoparticles, such as Cadmium Telluride ($CdTe$) and Carbon (C), have revolutionized the landscape of materials science, presenting tantalizing prospects for tailoring the properties of nanofluids to suit specific engineering needs. Their integration into nanofluid matrices holds promise for unlocking unprecedented levels of thermal and optical performance, thereby reshaping the boundaries of possibility across various domains, from energy conversion to medical diagnostics. In tandem with these advancements, numerical techniques like the Keller box method have emerged as indispensable tools for simulating and analysing fluid dynamics problems, providing researchers with the means to unravel the intricacies of complex systems in a controlled environment. Ahmad *et al.*[1] discussed the electromagnetohydrodynamics method using cadmium telluride ($CdTe$) and graphite (C) nanoparticles. Sheikh *et al.*[2] investigated the MHD flow of the Casson fluid containing cadmium telluride ($CdTe$) nanoparticle using the generalised Fourier's law. Jyotshna *et al.*[3] discussed the effect of activated radiation and heat source/sink on 3D Flow of Williamson nanoflow across a stretching sheet.

Heat loss or heat gain in a fluid flow process occurs always and it is an inevitable factor when we study energy transfer system in a boundary layer theory. Quite good examples of these situations are in building designs, in computers, the CPU, electronic circuits, etc. This energy generation concept is to enhance the fluid conductivity whilst the other reduces fluid energy. This term is inevitable only when there finds a huge temperature difference and because of this property, energy generation/absorption has greater importance in MHD flows. While the applications of magnetism in brain function (neurobiology) are still being explored, there's growing evidence that it plays a critical role in energy generation and absorption within the brain.

These applications were well discussed by the researchers in their early works[4-6]. Konda *et al.*[7] studied the variable heat sink/source on non-Newtonian fluid. Jyotshna *et al.*[8] extended the same effect over gallium nitride Williamson flow. Song *et al.*[9] investigated the same effects on stretched cylinder. Swain *et al.*[10] performed the same investigation in a porous medium.

Fluids embedded in a porous medium has vital role in many situations such as blending polymers, absorbent rocks, foams, aerogels etc. A prime example of the vital role fluids play in porous media is their function in lubrication and non-Newtonian batch mixers. Many researchers are interested in MHD flow submerged in a porous media because of its many applications, including drilling operations embedded in fluids, geothermal extractions, and boundary layer control in aerodynamics. Hamdan *et al.*[11] studied MHD flow embedded in a porous medium. Christian *et al.*[12] and Acharya *et al.*[13] considered a porous plate imbedded in an absorbent media. Veera *et al.*[14] investigated a semi-infinite strip under porous medium. Raghunath *et al.*[15] investigated studying the impacts of energy and species transfer in a permeable media amid plates. Mishra *et al.*[16] considered the impacts of heat source and radiation of a micropolar flow imbedded in a non-Darcy porous medium.

Naqvi *et al.*[17] explored hybrid nanoflow with heat radiation using numerical methods. Raza *et al.*[18] investigated Graphite nano thermodynamic system with Newtonian warming and sliding implications. Ahmad *et al.*[19] examined heat activation in the convective unidirectional flow of magnetised nanofluid hybrids. Sheikh *et al.*[20] investigated the transfer of heat acceleration caused by composite nanoparticles implanted in sodium alginate. Ghani *et al.*[21] investigated graphene-SWCNT nanoparticles over a Riga curved surface. Waqas *et al.*[22] considered a stretched sheet under a combination of nanofluid circulation with radiant heat.

The idea of radiation and convective heat transfer originates from the phenomena of oscillations propagating in every direction. Based on the energy carried by the particles, radiation is classified as ionized and non-ionized. Radiation has wide range of application in designing space craft, equipment design, smoke detectors, carbon dating techniques and so on. Hong *et al.*[23] explained how ultraviolet B rays emitted from the sun shattered through the outer layer of cells. Khan *et al.*[24] considered the thermal radiation to evaluate the properties of a dipole magnetic field with shear-thinning Williamson nanofluid. Mishra *et al.*[25] explored Williamson flow of hydromagnetic nanofluid technology flow over an expanding media considering radiative conditions.

Thus, with above knowledge, it is seen that very poor attention is paid on Williamson nanoflow past a circular cylinder in the presence of non-linear energy generation/absorption immersed in a porous medium. This fluid flow problem is solved by implicit Keller box method with non-similarity variables. The physical explanations of the numerical findings on the flow field are explained in depth using the diagrams.

Experimental Section

Problem statement

The geometry of the flow field is schematically depicted in Fig. 1. A time-independent, two-dimensional, Williamson fluid model past a horizontal cylinder is taken for study. Two nanoparticles *CdTe* and *C* with water as base are considered. Flow field is under the involvement of unidirectional radiation and the flow field is prone to heat production/lost. The flow field could be well described in the way that the x-axis is along the circumference of the horizontal cylinder and y-axis is normal to the surface. Radius of the horizontal cylinder is denoted by 'a' with gravity acting downwards. Boussinesq approximation holds since density variation is observed. Initially, the temperature of the surface of the cylinder and the nanofluid is maintained constant. Then the outside surface exchanges heat due to convection with a heat transfer coefficient T_f and unknown ambient

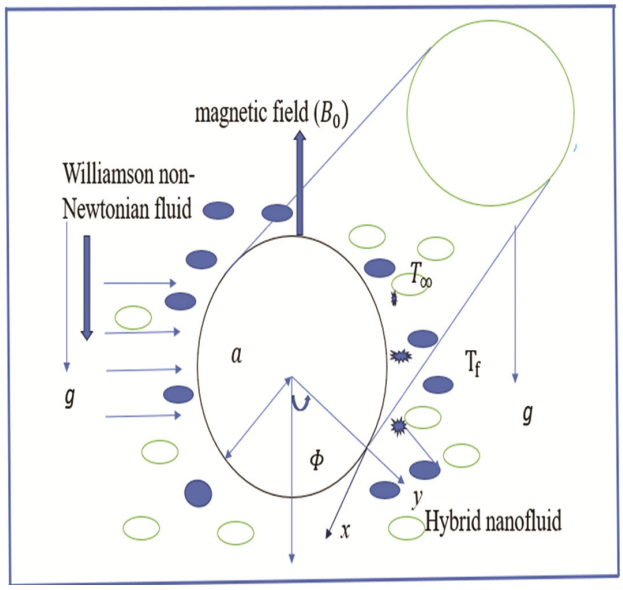

Fig. 1 — Coordinate system of geometry.

temperature T_∞. Homogeneous porous medium is assumed with a permeability parameter (K).

With the usual Bousinessq and boundary layer approximations, the equations for mass continuity and the conservation of momentum, energy, can be written as follows (Rao *et al.* [26]):

The continuity (1), momentum (2), energy (3) equation are defined as follows:

$$\frac{\partial u}{\partial x}+\frac{\partial v}{\partial y}=0,\ldots \quad \ldots (1)$$

$$u\frac{\partial u}{\partial x}+v\frac{\partial u}{\partial y}=\frac{\mu_{hnf}}{\rho_{hnf}}\frac{\partial^2 u}{\partial y^2}+\frac{\mu_{hnf}}{\rho_{hnf}}\sqrt{2v}\,\Gamma\frac{\partial u}{\partial y}\frac{\partial^2 u}{\partial y^2}+g\beta\left(T-T_\infty\right)\sin\left(\frac{x}{a}\right) \ldots (2)$$

$$-\frac{\sigma_{hnf}}{\rho_{hnf}}B_0 u-\frac{\mu_{hnf}}{\rho_{hnf}}\frac{u}{K}-\Gamma u^2,$$

$$u\frac{\partial T}{\partial x}+v\frac{\partial T}{\partial y}=\alpha_{hnf}\left(\frac{\partial^2 T}{\partial y^2}\right)+\frac{q'''}{\left(\rho c_p\right)_{hnf}}-\frac{1}{\left(\rho c_p\right)_{hnf}}\frac{\partial q_r}{\partial y}. \quad \ldots (3)$$

Where:

$$q'''=\frac{ku_w}{vx}\left(\left(f'\left(T_f-T_\infty\right)A\right)+\left(B\left(T-T_\infty\right)\right)\right). \quad \ldots (4)$$

The associated boundary conditions assumed for the study is as follows:

$$\left.\begin{aligned} &At\ y=0;\\ &\quad u=0,\ \ v=0,\\ &-k_{hnf}\frac{\partial T}{\partial y}=h\left(T_f-T\right).\\ &At\ \ y\to\infty;\\ &\quad u\to 0,\ \ v\to 0,\ T\to T_\infty. \end{aligned}\right\} \quad \ldots (5)$$

We introduce a stream function defined by the Cauchy-Riemann equations, $u=\left(\frac{\partial\psi}{\partial y}\right)$ and $v=-\left(\frac{\partial\psi}{\partial x}\right)$ and therefore, the mass conservation equation (1) is automatically satisfied.

For optically thick fluids, the proposed Rosseland heat approximation is used.

$$q_r=-\frac{4\sigma^*}{3k^*}\frac{\partial T^4}{\partial y} \quad \ldots . (6)$$

Expanding T^4 in Eq. (6) as Taylor series about the point T^4 (as a linear function), we have

$$T^4=4TT_\infty^3-3T_\infty^4, \quad \ldots . (7)$$

Substituting Eqns. (6)-(7) in Eq. (3) gives rise to the following form.

$$u\frac{\partial T}{\partial x}+v\frac{\partial T}{\partial y}=\alpha_{hnf}\frac{\partial^2 T}{\partial y^2}+\frac{ku_w}{vx}\begin{pmatrix}f'\left(T_f-T_\infty\right)A+\\ B\left(T-T_\infty\right)\end{pmatrix}+\frac{16\sigma^*T_\infty^3}{3k^*\rho c_p}\frac{\partial^2 T}{\partial y^2}. \quad \ldots (8)$$

The following nondimensional quantities are added to formulate dimensionless governing equations and boundaries.

$$\left.\begin{aligned} &\xi=\frac{x}{a},\quad \eta=\frac{y}{a}\sqrt[4]{Gr},\\ &f\left(\xi,\eta\right)=\frac{\psi}{v\,\xi\sqrt[4]{Gr}},\ \ \mathrm{Pr}=\frac{v}{\alpha},\\ &Gr=\frac{g\beta\left(T_f-T_\infty\right)}{v^2},\\ &\theta\left(\xi,\eta\right)=\frac{T-T_\infty}{T_f-T_\infty},M=\frac{\sigma B_0^2a^2}{\rho v\sqrt{Gr}},\\ &We=\frac{\sqrt{2v}\ \Gamma\xi\,Gr^{(3/4)}}{a^2}. \end{aligned}\right\} \quad \ldots (9)$$

Considering equation (9), equations (2) to (4) are reduced to the coupled, nonlinear, Domain-specific without dimensions partial differential equations for energy as well as momentum equations:

$$\zeta_1 f''' + f f'' - (1+\xi\Lambda)(f')^2 + \zeta_1 We f'' f''' + \frac{\sin\xi}{\xi}\theta - \zeta_2\left(M+\frac{1}{Da}\right)f' = \xi\left(f'\frac{\partial f'}{\partial \xi} - f''\frac{\partial f}{\partial \xi}\right). \quad \text{.... (10)}$$

$$\frac{1}{\Pr}\left(1+\frac{4}{3F}\right)\theta''\zeta_3 + f\theta' + A f + B\theta = \xi\left(f'\frac{\partial\theta}{\partial\xi} - \theta'\frac{\partial f}{\partial\xi}\right). \quad \text{.... (11)}$$

Where:

$$M^* = \frac{A^* k (Gr)^{1/2}}{g\beta(T_f - T_\infty)},\ N^* = \frac{B^* k (Gr)^{1/2}}{g\beta(T_f - T_\infty)}.$$

The dimensionless flow boundary conditions are below:

$$At\ \eta = 0;\quad f = 0,\ f' = 0,\ \frac{k_{hnf}}{k_f}\theta'(\eta) = -Bi(1-\theta(\eta)),$$
$$As\ \eta \to \infty;\ f' \to 0,\quad \theta \to 0. \quad \text{... (12)}$$

Two terms related to engineering are the skin-friction coefficient and the Nusselt number. design parameters of physical importance.

$$\frac{1}{2}C_f Gr^{-3/4} = \left(1.0+\frac{1}{\beta}\right)\frac{\mu_{thnf}}{\mu_f}\xi f''(0) \quad \text{... (13)}$$

$$Nu\ Gr^{-1/4} = -\frac{k_{thnf}}{k_f}\left(1+\frac{4}{3F}\right)\theta'(0) \quad \text{.... (14)}$$

Thermophysical as well as rheological property (Ahmad *et al.*[1])

(1). Density

$$\rho_{hnf} = \psi_1\rho_{p1} + \psi_2\rho_{p2} + (1-\psi_1-\psi_2)\rho_f,$$

$$(\rho C_p)_{hnf} = \psi_1(\rho C_p)_{p1} + \psi_2(\rho C_p)_{p2} + (1-\psi_1-\psi_2)(\rho C_p)_f,$$

(2). Viscosity

$$\frac{\mu_{hnf}}{\mu_{bf}} = 1 + 14.6\psi_2 + 123.3\psi_2^2$$

$$\frac{\mu_{bf}}{\mu_f} = 1 + 14.6\psi_1 + 123.3\psi_1^2$$

(3). Thermal conductivity

$$\frac{k_{hnf}}{k_{bf}} = \frac{(k_{p2}+7.26k_{bf}) + 7.26\psi_2(k_{p2}-k_{bf})}{(k_{p2}+7.26k_{bf}) - \psi_2(k_{p2}-k_{bf})},$$

$$\frac{k_{bf}}{k_f} = \frac{(k_{p1}+7.26k_f) + 7.26\psi_1(k_{p1}-k_f)}{(k_{p1}+7.26k_f) - \psi_1(k_{p1}-k_f)},$$

(4). Electrical conductivity

$$\frac{\sigma_{hnf}}{\sigma_{bf}} = 1 + \frac{3\left(\left(\sigma_{p2}/\sigma_{bf}\right)-1\right)\psi_2}{\left(\sigma_{p2}/\sigma_{bf}\right)+2-\left(\left(\sigma_{p2}/\sigma_{bf}\right)-1\right)\psi_2}$$

$$\frac{\sigma_{bf}}{\sigma_f} = 1 + \frac{3\left(\left(\sigma_{p1}/\sigma_f\right)-1\right)\psi_1}{\left(\sigma_{p1}/\sigma_f\right)+2-\left(\left(\sigma_{p}/\sigma_f\right)-1\right)\psi_1}$$

Where:

$$\zeta_1 = \frac{(1+14.6\psi_2+123.3\psi_2^2)(1+14.6\psi_1+123.3\psi_1^2)}{(\psi_1(\rho_{p1}/\rho_f)+\psi_2(\rho_{p2}/\rho_f)+(1-\psi_1-\psi_2))},$$

$$\zeta_2 = \frac{\left(1+\begin{pmatrix}3\left((\sigma_{p1}/\sigma_f)-1\right)\psi_1/(\sigma_{p1}/\sigma_f)\\ +2-\left((\sigma_{p1}/\sigma_f)-1\right)\psi_1\end{pmatrix}\right)}{\psi_1(\rho_{p1}/\rho_f)+\psi_2(\rho_{p2}/\rho_f)+(1-\psi_1-\psi_2)},$$

$$\left(1+\begin{pmatrix}3\left((\sigma_{p2}/\sigma_{bf})-1\right)\psi_2/(\sigma_{p2}/\sigma_{bf})\\ +2-\left((\sigma_{p2}/\sigma_{bf})-1\right)\psi_2\end{pmatrix}\right)$$

$$\zeta_3 = \frac{\begin{pmatrix}\left(k_{p2}+7.26k_{bf}\right)+7.26\psi_2\left(k_{p2}-k_{bf}\right)/\\ \left(k_{p2}+7.26k_{bf}\right)-\psi_2\left(k_{p2}-k_{bf}\right)\end{pmatrix}}{\begin{pmatrix}\left(k_{p1}+7.26k_f\right)+7.26\psi_1\left(k_{p1}-k_f\right)/\\ \left(k_{p1}+7.26k_f\right)-\psi_1\left(k_{p1}-k_f\right)\end{pmatrix}}{\psi_1\left(\left(\rho C_p\right)_{p1}/\left(\rho C_p\right)_f\right)+\psi_2\left(\left(\rho C_p\right)_{p2}/\left(\rho C_p\right)_f\right)+\left(1-\psi_1-\psi_2\right)},$$

Keller-box implicit method (numerical finite difference solution)

An accurate, completely efficient, and stable Keller-box method is utilised for the computational solution of the dimensionless boundary layer equations since it combines second-degree validity with the ability of step size adaptation. Since its quicker convergence rate relative to conventional numerical techniques, this approach is best suited for solving boundary layer flow problems. Using this approach, higher-order PDEs are reduced to first order PDEs, which are then translated into central difference formulas. The decomposition of LU technique is used to solve the matrix-vector form of transformed solutions. The material domain $(0,\infty)$ is used throughout the computation procedure is condensed to the limited area $[\eta_0,\eta_\infty]$ by altering $\eta_0=0,\eta_\infty=20,\eta_p=1000$ and $h=\frac{\eta_\infty-\eta_0}{\eta_p}$ to establish the initial approximations of the computerised solution. Increasingthe total amount of points on the grid by decreasing the step size h helps to attain the necessary precision of ε^{-6}. A process diagram (Fig. 2) depicts the whole explanation of the Keller-Box simulation/numerical code.

Step 1: The Nth order partial differential equation system reduced to N first-order equations.

We add the most recent set of variables listed below to convert higher-order PDEs to first order PDEs:$p_1(\xi,\eta),p_2(\xi,\eta),p_3(\xi,\eta)$

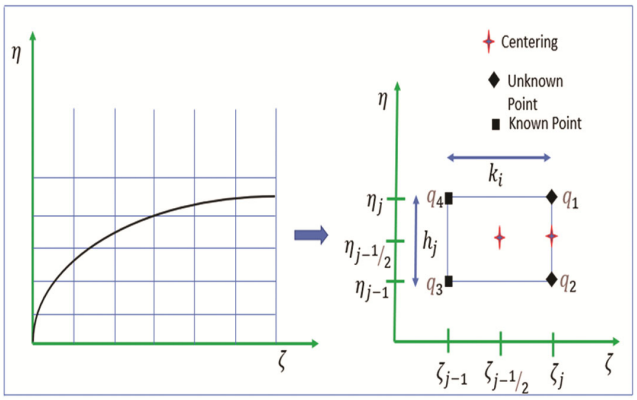

Fig. 2 — Keller box element and boundary layer mesh image

$$,p_4(\xi,\eta),p_5(\xi,\eta).$$

$$\begin{aligned}&f=f,f'=p_1,p_1'=p_2,\theta=p_3,p_3'=p_4,\\&f=f,f'=p_1,f''=p_2,f'''=p_2'\\&\theta=p_3,\theta'=p_4,\theta''=p_4'\\&\psi_1\left(p_2'\right)+We\,\psi_1\left(p_2p_2'\right)+\left(fp_2\right)\\&-\left(1+\zeta*\Lambda\right)\left(p_1\right)^2+\frac{\sin\zeta}{\zeta}(\theta)\\&-\psi_2\left(M+\frac{1}{Da}\right)(p_1)\\&=\zeta\left(p_1\frac{\partial p_1}{\partial\zeta}-p_2\frac{\partial f}{\partial\zeta}\right)\end{aligned} \quad \text{.... (16)}$$

$$\begin{aligned}&\frac{1}{\Pr}\left(1+\frac{4}{3F}\right)\left(p_4'\right)\psi_3+\left(f\,p_4\right)\\&+A(p_1)+B(p_3)\\&=\zeta\left(p_1\frac{\partial p_3}{\partial\zeta}-p_4\frac{\partial f}{\partial\xi}\right)\end{aligned} \quad \text{... (17)}$$

Boundary condition becomes.

$$\begin{aligned}&\eta=0\ :p_1=0,f=0,p_3=1+\frac{1}{Bi}p_4\\&\eta\to0:p_1\to0,p_3\to0.\end{aligned} \quad \text{... (18)}$$

Step 2: The finite difference method

The rectangular net is in the x and y planes, as shown in Fig. 2, and the following are the net points:

$$\begin{aligned}&\zeta^0=0,\zeta^n=\zeta^{n-1}+k_n,n=1,2,...,I\\&\eta_0=0,\ \eta_j=\eta_{j-1}+h_j,j=1,2,...,J\end{aligned} \quad \text{.... (19)}$$

Where k_n and h_j represent the $\Delta\xi$ and $\Delta\eta$ spacing, respectively.

$$\begin{aligned}&\left(\frac{\partial(\ )}{\partial\zeta}\right)_{n-\frac{1}{2}}^{n-\frac{1}{2}}=\frac{(\ )_{j-\frac{1}{2}}^{n}-(\ )_{j-\frac{1}{2}}^{n-1}}{k_n}\\&\left(\frac{\partial(\ )}{\partial\eta}\right)_{j-\frac{1}{2}}^{n-\frac{1}{2}}=\frac{(\ )_{j-\frac{1}{2}}^{n}-(\ )_{j-\frac{1}{2}}^{n-1}}{h_j}\\&(\ )_j^{n-\frac{1}{2}}=\frac{(\ )_j^{n-1}-(\ )_j^{n}}{2},\\&(\ )_{j-\frac{1}{2}}^{n}=\frac{(\ )_{j-1}^{n}-(\ )_j^{n}}{2}\end{aligned} \quad \text{... (20)}$$

The finite-difference form is computed using the central difference technique.

$$f' = p_1 \Rightarrow (p_1)^n_{j-\frac{1}{2}} = \frac{(p_1)^n_j + (p_1)^n_{j-1}}{2} = \frac{\left(f^n_j - f^n_{j-1}\right)}{h_j}$$

$$(p_1)' = p_2 \Rightarrow (p_2)^n_{j-\frac{1}{2}} = \frac{(p_2)^n_j + (p_2)^n_{j-1}}{2} = \frac{\left((p_1)^n_j - (p_1)^n_{j-1}\right)}{h_j}$$

$$(p_1)' = p_4 \Rightarrow (p_4)^n_{j-\frac{1}{2}} = \frac{(p_4)^n_j + (p_4)^n_{j-1}}{2} = \frac{\left((p_3)^n_j - (p_3)^n_{j-1}\right)}{h_j} \quad \text{.... (21)}$$

The following equations (21) are centred at the $(\xi^{i-\frac{1}{2}},\ \eta_{j-\frac{1}{2}})$ locations, which are shown below.

$$\psi_1\left(\frac{(p_2)^n - (p_2)^{n-1}_{j-1}}{h_j}\right) + (1+\alpha)\left(f^n_{j-\frac{1}{2}}\right)\left(q^n_{j-\frac{1}{2}}\right) - (1+\alpha+\zeta*\Lambda)\left((p_1)^n_{j-\frac{1}{2}}\right)^2 + A\left((p_3)^n_{j-\frac{1}{2}}\right) + We\,\psi_1\left((p_2)^n_{j-\frac{1}{2}}\right)\left(\frac{(p_2)^n - (p_2)^{n-1}_{j-1}}{h_j}\right) - \left(M+\frac{1}{Da}\right)\psi_2\left((p_1)^n_{j-\frac{1}{2}}\right) - \alpha f^{n-1}_{j-\frac{1}{2}}\left((q_2)^n_{j-\frac{1}{2}}\right) + \alpha\left((p_2)^{n-1}_{j-\frac{1}{2}}\right)\left(f^n_{j-\frac{1}{2}}\right)$$

$$= \begin{bmatrix} \left(\frac{(p_2)_j - (p_2)_{j-1}}{h_j}\right)\psi_1 + (1-\alpha)\left(f^n_{j-\frac{1}{2}}\right)\left((p_2)^n_{j-\frac{1}{2}}\right) \\ + We\,(p_2)^n_{j-\frac{1}{2}}\,(p_2')^n_{j-\frac{1}{2}}\,\psi_1 + (1-\alpha-\Lambda*\zeta)\left((p_1)_{j-\frac{1}{2}}\right)^2 \\ + A\left((p_3)^n_{j-\frac{1}{2}}\right) - \left(M+\frac{1}{Da}\right)\left((p_1)_{j-\frac{1}{2}}\right)\psi_2 \end{bmatrix} \quad \text{... (22)}$$

$$\frac{1}{\Pr}\left(1+\frac{4}{3F}\right)\psi_3\left(\frac{(p_4)^n_j - (p_4)^n_{j-1}}{h_j}\right) + (1+\alpha)\left(f^n_{j-\frac{1}{2}}\right)(p_4)^n_{j-\frac{1}{2}} - \alpha\left[(p_1)^n_{j-\frac{1}{2}}(p_3)^n_{j-\frac{1}{2}}\right] + \alpha\left((p_3)^{n-1}_{j-\frac{1}{2}}\right)\left((p_1)^n_{j-\frac{1}{2}}\right) - \alpha(p_1)^{n-1}_{j-\frac{1}{2}}(p_3)^n_{j-\frac{1}{2}} - \alpha f^{n-1}_{j-\frac{1}{2}}\left((p_4)^n_{j-\frac{1}{2}}\right) + \alpha(p_4)^{n-1}_{j-\frac{1}{2}}\left(f^n_{j-\frac{1}{2}}\right) + M\left((p_1)^n_{j-\frac{1}{2}}\right) + N\left((p_3)^n_{j-\frac{1}{2}}\right)$$

$$= -\begin{bmatrix} \frac{1}{\Pr}\left(1+\frac{4}{3F}\right)\left(\frac{\left(P^n_4\right)_j - \left(p^n_4\right)_{j-1}}{h_j}\right)\psi_3 + \\ (1-\alpha)\left(f^n_{j-\frac{1}{2}}\right)(p_4)^n_{j-\frac{1}{2}} + \alpha\left((p_1)^n_{j-\frac{1}{2}}(p_3)^n_{j-\frac{1}{2}}\right) \\ + M\left((p_1)^n_{j-1/2}\right) + N\left((p_3)^n_{j-\frac{1}{2}}\right) \end{bmatrix} \quad \text{.... (23)}$$

Where:

$$\alpha = \frac{\xi^{n-1/2}}{k_n}, \qquad B = \frac{\sin\left(\xi^{n-1/2}\right)}{\xi^{n-1/2}}$$

The boundary conditions,

$$\left.\begin{aligned} f^n_0 = (p_1)^n_0 = 0, (p_3)^n_0 = 1 + \frac{1}{\beta_1}(p_4)^n_0 \\ (p_1)^n_J \to 1,\ (p_3)^n_J = 0 \end{aligned}\right\} \quad \text{... (24)}$$

Step 3: Newton's linearization approach

Using well-known techniques[31] $(f^{n-1}_j, (p_1)^{n-1}_j, (p_2)^{n-1}_j, (p_3)^{n-1}_j, (p_4)^{n-1}_j, (p_5)^{n-1}_j)$ the unknown $(f^n_j, (p_1)^n_j, (p_2)^n_j, (p_3)^n_j, (p_4)^n_j, (p_5)^n_j)$ are predicted to be $0 \le j \le J$.

$$\left(f^n_j, (p_1)^n_j, (p_2)^n_j, (p_3)^n_j, (p_4)^n_j\right) \equiv \left(f_j, (p_1)_j, (p_2)_j, (p_3)_j, (p_4)_j\right).$$

The collection of Equations of central difference is denoted as

$$\frac{(p_1)_j + (p_1)_{j-1}}{2} = \frac{f_j - f_{j-1}}{h_j} \quad \text{... (25)}$$

$$\frac{(p_2)_j + (p_2)_{j-1}}{2} = \frac{(p_1)_j - (p_1)_{j-1}}{h_j} \quad \text{.... (26)}$$

$$\frac{(p_4)_j + (p_4)_{j-1}}{2} = \frac{(p_3)_j - (p_3)_{j-1}}{h_j} \quad \text{... (27)}$$

$$\frac{(p_6)_j + (p_6)_{j-1}}{2} = \frac{(p_5)_j - (p_5)_{j-1}}{h_j} \quad \text{.... (28)}$$

$$\begin{aligned}
&\psi\left((p_2)_j - (p_2)_{j-1}\right) + \\
&(1+\alpha)\frac{h_j}{4}\left[\left(f_j + f_{j-1}\right)\left((p_2)_j + (p_2)_{j-1}\right)\right] \\
&+\frac{A^* h_j}{2}\left((p_3)_j + (p_3)_{j-1}\right) \\
&-(1+\alpha+\varepsilon * \Lambda)\frac{h_j}{4}\left((p_1)_j + (p_1)_{j-1}\right)^2 \\
&+\frac{We}{2}\psi_1\left((p_2)_j + (p_2)_{j-1}\right)\left((p_2)_j - (p_2)_{j-1}\right) \\
&-\left(M + \frac{1}{Da}\right)\frac{h_j}{2}\psi_2\left((p_1)_j + (p_1)_{j-1}\right) \\
&-\frac{\alpha h_j}{2} f_{j-\frac{1}{2}}^{n-1}\left((p_2)_j + (p_2)_{j-1}\right) \\
&+\frac{\alpha h_j}{2}(p_2)_{j-\frac{1}{2}}^{n-1}\left(f_j + f_{j-1}\right) = \left[\Pi_1\right]_{j-\frac{1}{2}}^{n-1}
\end{aligned} \quad \text{... (29)}$$

$$\begin{aligned}
&\frac{1}{\Pr}\left(1+\frac{4}{3F}\right)\psi_3\left((p_4)_j - (p_4)_{j-1}\right) + \\
&(1+\alpha)\frac{h_j}{4}\left(f_j + f_{j-1}\right)\left(t_j + t_{j-1}\right) \\
&-\frac{\alpha h_j}{4}\left[\left((p_1)_j + (p_1)_{j-1}\right)\left((p_3)_j - (p_3)_{j-1}\right)\right] + \\
&\frac{\alpha h_j}{2}(p_3)_{j-\frac{1}{2}}^{n-1}\left((p_1)_j + (p_1)_{j-1}\right) \\
&-\frac{\alpha}{2}h_j\,(p_1)_{j-\frac{1}{2}}^{n-1}\left((p_3)_j + (p_3)_{j-1}\right) - \\
&\frac{\alpha h_j}{2} f_{j-\frac{1}{2}}^{n-1}\left((p_4)_j + (p_4)_{j-1}\right) + \\
&\frac{\alpha h_j}{2}(p_4)_{j-\frac{1}{2}}^{n-1}\left(f_j + f_{j-1}\right) \\
&+M\left((p_1)_{j-\frac{1}{2}}^{n}\right) + N\left((p_3)_{j-\frac{1}{2}}^{n}\right) = \left[\Pi_2\right]_{j-\frac{1}{2}}^{n-1}
\end{aligned} \quad \text{.... (30)}$$

$$\left[\Pi_1\right]_{j-\frac{1}{2}}^{n-1} = -h_j \begin{bmatrix} \left(\frac{(p_2)_j - (p_2)_{j-1}}{h_j}\right)\psi_1 + \\ (1-\alpha)\left(\left(f_{j-\frac{1}{2}}\right)(p_2)_{j-\frac{1}{2}}\right) \\ +(1-\alpha-\Lambda\varepsilon)\left((p_1)_{j-1/2}\right)^2 \\ +We\ (p_2)_{j-\frac{1}{2}}\left(\frac{(p_2)_j - (p_2)_{j-1}}{h_j}\right)\psi_1 \\ +A^*\left((P_3)_{j-\frac{1}{2}}\right) - \left(M + \frac{1}{Da}\right)\left((p_1)_{j-\frac{1}{2}}\right)\psi_2 \end{bmatrix} \quad \text{.... (31)}$$

$$\left[\Pi_2\right]_{j-\frac{1}{2}}^{n-1} = -h_j \begin{bmatrix} \frac{1}{\Pr}\left(1+\frac{4}{3F}\right)\left(\frac{(p_4)_j - (p_4)_{j-1}}{h_j}\right)\psi_3 \\ +(1-\alpha)\left(f_{j-\frac{1}{2}}\right)(p_4)_j \\ +\alpha\left((p_1)_{j-\frac{1}{2}}(p_3)_{j-\frac{1}{2}}\right) + \\ M(p_1)_{j-\frac{1}{2}} + N(p_3)_{j-\frac{1}{2}} \end{bmatrix} \quad \text{.... (32)}$$

Where $[\Pi_1]_{j-1/2}^{n-1}$, $[\Pi_2]_{j-1/2}^{n-1}$ are the known quantities.

The iterates used below helps in transforming the nonlinear system of algebraic equations to linear by means of Newton's method.

$$\Delta f_j^{(n)} + f_j^n = f_j^{(n+1)} \quad \text{.... (33)}$$

$$\Delta(p_1)_j^{(n)} + (p_1)_j^{(n)} = (p_1)_j^{(n+1)} \quad \text{... (34)}$$

$$\Delta(p_2)_j^{(n)} + (p_2)_j^{(n)} = (p_2)_j^{(n+1)} \quad \text{.... (35)}$$

$$\Delta(p_3)_j^{(n)} + (p_3)_j^{(n)} = (p_3)_j^{(n+1)} \quad \text{... (36)}$$

$$\Delta(p_4)_j^{(n)} + (p_4)_j^{(n)} = (p_4)_j^{(n+1)} \quad \text{.... (37)}$$

The system of Eqs (33)-(37) enforced in Eqs (25)-(32) with the higher-order of (Δ) removed.

$$\begin{aligned}
&\Delta f_j - \Delta f_{j-1} - \frac{h_j}{2}\Delta(p_1)_j - \\
&\frac{h_j}{2}\Delta(p_1)_{j-1} - (l_1)_j = 0
\end{aligned} \quad \text{.... (38)}$$

$$\Delta(p_1)_j - \Delta(p_1)_{j-1} - \frac{h_j}{2}\Delta(p_2)_j - \frac{h_j}{2}\Delta(p_2)_{j-1} - (l_2)_j = 0 \quad \text{.... (39)}$$

$$\Delta(p_3)_j - \Delta(p_3)_{j-1} - \frac{h_j}{2}\Delta(p_4)_j - \frac{h_j}{2}\Delta(p_4)_{j-1} - (l_3)_j = 0 \quad \text{.... (40)}$$

$$(G_1)_j \Delta(p_2)_j + (G_2)_j \Delta(p_2)_{j-1} + (G_3)_j \Delta f_j + (G_4)_j \Delta f_{j-1} + (G_5)_j \Delta(p_1)_j + (G_6)_j \Delta(p_1)_{j-1} + (G_7)_j \Delta(p_3)_j + (G_8)_j \Delta(p_3)_{j-1} - (l_4)_j = 0 \quad \text{....(41)}$$

$$(H_1)_j \Delta(p_4)_j + (H_2)_j \Delta(p_4)_{j-1} + (H_3)_j \Delta(f_j) + (H_4)_j \Delta(f_{j-1}) + (H_5)_j \Delta(p_1)_j + (H_6)_j \Delta(p_1)_{j-1} + (H_7)_j \Delta(p_3)_j + (H_8)_j \Delta(p_3)_{j-1} - (l_5)_j = 0 \quad \text{.... (42)}$$

Where:

$$G_1 = \left(1 + We\frac{h_j}{2}\left(p_{j-\frac{1}{2}}\right)\right)\psi_1 + (1+\alpha)\frac{h_j}{2}\left(f_{j-\frac{1}{2}}\right) - \frac{\alpha h_j}{2} f^{n-1}_{j-\frac{1}{2}}$$

$$G_2 = -\left(1 + We\frac{h_j}{2}\left(p_{j-\frac{1}{2}}\right)\right)\psi_1 + (1+\alpha)\frac{h_j}{2}\left(f_{j-\frac{1}{2}}\right) - \frac{\alpha h_j}{2} f^{n-1}_{j-\frac{1}{2}}$$

$$G_3 = \frac{(1+\alpha)h_j}{2}(p_2)_{j-\frac{1}{2}} + \frac{\alpha h_j}{2}(p_2)^{n-1}_{j-\frac{1}{2}}$$

$$G_4 = \frac{(1+\alpha)h_j}{2}(p_2)_{j-\frac{1}{2}} + \frac{\alpha h_j}{2}(p_2)^{n-1}_{j-\frac{1}{2}}$$

$$G_5 = -(1+\alpha+\varepsilon * \Lambda)\frac{h_j}{2}(p_1)_{j-\frac{1}{2}} - \left(M + \frac{1}{Da}\right)\frac{h_j}{2}\psi_2$$

$$G_6 = -(1+\alpha+\varepsilon * \Lambda)\frac{h_j}{2}(p_1)_{j-\frac{1}{2}} - \left(M + \frac{1}{Da}\right)\frac{h_j}{2}\psi_2$$

$$G_7 = \frac{Ah_j}{2}$$

$$G_8 = \frac{Ah_j}{2}$$

$$H_1 = \frac{1}{\Pr}\left(1 + \frac{4}{3F}\right) - \frac{\alpha h_j}{2} f^{n-1}_{j-\frac{1}{2}} + (1+\alpha)\frac{h_j}{2} f_{j-\frac{1}{2}}$$

$$H_2 = \frac{1}{\Pr}\left(1 + \frac{4}{3F}\right) - \frac{\alpha h_j}{2} f^{n-1}_{j-\frac{1}{2}} + (1+\alpha)\frac{h_j}{2} f_{j-\frac{1}{2}}$$

$$H_3 = \frac{(1+\alpha)}{2} h_j (p_4)_{j-\frac{1}{2}} + \frac{\alpha h_j}{2}(p_4)^{n-1}_{j-\frac{1}{2}}$$

$$H_4 = \frac{(1+\alpha)}{2} h_j (p_4)_{j-\frac{1}{2}} + \frac{\alpha h_j}{2}(p_4)^{n-1}_{j-\frac{1}{2}}$$

$$H_5 = -\frac{\alpha h_j}{2}(p_3)_{j-\frac{1}{2}} + \frac{\alpha h_j}{2}(p_3)^{n-1}_{j-\frac{1}{2}} + M\frac{h_j}{2}$$

$$H_6 = -\frac{\alpha h_j}{2}(p_3)_{j-\frac{1}{2}} + \frac{\alpha h_j}{2}(p_3)^{n-1}_{j-\frac{1}{2}} + M\frac{h_j}{2}$$

$$H_7 = -\frac{\alpha h_j}{2}(p_1)_{j-\frac{1}{2}} - \frac{\alpha h_j}{2}(p_1)^{n-1}_{j-\frac{1}{2}} + N\frac{h_j}{2}$$

$$H_8 = -\frac{\alpha h_j}{2}(p_1)_{j-\frac{1}{2}} - \frac{\alpha h_j}{2}(p_1)^{n-1}_{j-\frac{1}{2}} + N\frac{h_j}{2}$$

$$[l_4] = \psi_1\left((p_2)_{j-1} - (p_2)\right) - (1+\alpha)\frac{h_j}{4}\left(f_{j-\frac{1}{2}}\right)(p_2)_{j-\frac{1}{2}} + (1+\alpha+\varepsilon\Lambda)\frac{h_j}{4}(p_1)^2_{j-\frac{1}{2}} - \frac{A}{2}h_j(p_3)_{j-\frac{1}{2}} + We\psi_1(p_2)_{j-\frac{1}{2}}\left((p_2)_{j-1} - (p_2)_j\right) + \left(M + \frac{1}{Da}\right)\frac{h_j}{2}\psi_2(p_1)_{j-\frac{1}{2}} + \frac{\alpha h_j}{2} f^{n-1}_{j-\frac{1}{2}}(p_2)_{j-\frac{1}{2}} - \frac{\alpha h_j}{2}(p_2)^{n-1}_{j-\frac{1}{2}}\left(f_{j-\frac{1}{2}}\right) + [\Pi_1]^{n-1}_{j-\frac{1}{2}} \quad \text{... (43)}$$

$$[l_5] = \frac{1}{\Pr}\left(1 + \frac{4}{3F}\right)\left((p_4)_{j-1} - (p_4)_j\right) - (1+\alpha)h_j\left(\left(f_{j-\frac{1}{2}}\right)(p_4)_{j-\frac{1}{2}}\right) + \alpha h_j\left((p_1)_{j-\frac{1}{2}}(p_3)_{j-\frac{1}{2}}\right) - \alpha h_j(p_3)^{n-1}_{j-\frac{1}{2}}(p_1)_{j-\frac{1}{2}} + \frac{\alpha h_j}{2}(p_1)^{n-1}_{j-\frac{1}{2}}(p_3)_{j-\frac{1}{2}} + \frac{\alpha h_j}{2} f^{n-1}_{j-\frac{1}{2}}(p_4)_{j-\frac{1}{2}} + \frac{\alpha h_j}{2}(p_4)^{n-1}_{j-\frac{1}{2}} f_{j-\frac{1}{2}} + h_j M\left((p_1)_{j-\frac{1}{2}}\right) + N h_j\left((p_3)_{j-\frac{1}{2}}\right) + [\Pi_2]^{n-1}_{j-\frac{1}{2}} \quad \text{... (44)}$$

With the boundary conditions

$$\left.\begin{aligned} &\Delta f_0^n = 0, \quad \Delta\left(p_1\right)_0^n = 0, \quad \Delta\left(p_3\right)_0^n = 0, \\ &\Delta\left(p_1\right)_J^n = 0, \Delta\left(p_3\right)_J^n = 0, \\ &f_0^n = \left(p_1\right)_0^n = 0, \left(\left(p_3\right)_0^1\right) = 1, \\ &\left(p_1\right)_J^n = 0, \left(p_3\right)_J^n = 0 \end{aligned}\right\} \quad \text{... (45)}$$

Step 4: Tridiagonal System of Solution

The block-elimination approach may be used to solve the linearized difference Eqs (38)-(45) by Cebeci and Bradshaw[27], because the system is block-tridiagonal in structure. The block-tridiagonal structure is often made up of variables or constants, but in this case, an unusual aspect is that it is made up of block matrices, Eqs (38)-(45) may be represented in matrix-vector form as

$$Q\,\Omega = l \quad \text{... (46)}$$

Where:

$$Q = \begin{bmatrix} [Q_1] & [R_1] & & & & \\ [R_2] & [Q_2] & [S_2] & & & \\ & \ddots & \ddots & \ddots & & \\ & & & & [R_{j-1}] & [Q_{j-1}] & [S_{j-1}] \\ & & & & [R_j] & [Q_j] \end{bmatrix}$$

$$\Omega = \begin{bmatrix} [\Omega_1] \\ [\Omega_2] \\ \vdots \\ [\Omega_{j-1}] \\ [\Omega_j] \end{bmatrix} \quad \textit{and} \quad l = \begin{bmatrix} [l_1] \\ [l_2] \\ \vdots \\ [l_{j-1}] \\ [l_j] \end{bmatrix}$$

The matrix components the following

Where:

$$-\frac{h_j}{2} = -z$$

$$|Q_1| = \begin{bmatrix} 0 & 0 & 1 & 0 & 0 \\ -z & 0 & 0 & -z & 0 \\ 0 & -z & 0 & 0 & -z \\ (G_2) & 0 & (G_3) & (G_1) & 0 \\ 0 & (H_2) & (H_3) & 0 & (H_1) \end{bmatrix}$$

For $J \geq j \geq 2$:

$$|Q_j| = \begin{bmatrix} -Z & 0 & 1 & 0 & 0 \\ -1 & 0 & 0 & -Z & 0 \\ 0 & -1 & 0 & 0 & -Z \\ (G_6) & (G_8) & (G_3) & (G_1) & 0 \\ (H_6) & (H_8) & (H_3) & 0 & (H_1) \end{bmatrix}, J \geq j \geq 2$$

$$|R_J| = \begin{bmatrix} 0 & 0 & -1 & 0 & 0 \\ 0 & 0 & 0 & -z & 0 \\ 0 & 0 & 0 & 0 & -z \\ 0 & 0 & (G_4) & (G_2) & 0 \\ 0 & 0 & (H_4) & 0 & (H_1) \end{bmatrix}, 2 \leq j \leq J$$

In the case $J-1 \geq j \geq 1$:

$$|S_J| = \begin{bmatrix} -z & 0 & 0 & 0 & 0 \\ 1 & 0 & 0 & 0 & 0 \\ 0 & 1 & 0 & 0 & 0 \\ (G_5) & (G_7) & 0 & 0 & 0 \\ (H_5) & (H_7) & 0 & 0 & 0 \end{bmatrix}, 2 \leq j \geq J$$

For the category $J \geq j \geq 2$:

$$[\Omega_1] = \begin{bmatrix} \Omega(p_1)_0 \\ \Omega(p_3)_0 \\ \Omega(f)_1 \\ \Omega(p_1)_1 \\ \Omega(p_2)_1 \end{bmatrix}, [\Omega_j] = \begin{bmatrix} \Omega(p_1)_{J-1} \\ \Omega(p_3)_{J-1} \\ \Omega(f)_J \\ \Omega(p_1)_J \\ \Omega(p_2)_J \end{bmatrix}$$

And $J \geq j \geq 1$:

$$[l_j] = \begin{bmatrix} (l_1)_{j-1/2} \\ (l_2)_{j-1/2} \\ (l_3)_{j-1/2} \\ (l_4)_{j-1/2} \\ (l_5)_{j-1/2} \end{bmatrix}$$

Table 1 — Comparison table showing the local heat transfer coefficient for the reduced cases$We = 0, Bi = 0, M = 0.0$

ξ	Pr =1.0 Nazar *et al.*[29]	Pr = 1.0 Subba Rao *et al.*[30]	Present solutions
0	0.4214	0.4212	0.4211
$\pi/6$	0.4161	0.4259	0.4257
$\pi/3$	0.4005	0.4004	0.4002
$\pi/2$	0.3741	0.4004	0.4001
$2\pi/3$	0.3355	0.3743	0.3740
$5\pi/6$	0.2811	0.2809	0.2808
π	0.1916	0.1917	0.1914

Table 2 — displays the thermophysical values for nanomaterials and base fluids. (Ahmad *et al.*[1])

Properties	Base fluid (H_2O)	Nanoparticles $CdTe$ (ψ_1)	Nanoparticles C (ψ_2)
Density (kgm^{-1})	997.1	5855	2060
Thermal conductivity $(Wm^{-1}K^{-1})$	0.613	7.5	25
Specific heat $(Jkg^{-1}K^{-1})$	4179	209.0	720
Electrical conductivity (Sm^{-1})	0.05	7.0×10^{-7}	5.0×10^{2}

The linearized solution system is transformed utilising the Thomas technique, into a block tridiagonal form (Cebeci and Bradshaw[27]). Regarding the calculation, the spatial nodes $(\xi)$and (η) are set to 0.05. To increase the correctness of the result, the convergence criteria as set (10^{-6}) in this present computation. Table 1 compares our current methodology results with existing literature Nazar *et al.*[29] and Subba Rao *et al.*[30] and found in good agreement.

Results and Discussion

The investigation on hybrid-class Cadmium telluride $(CdTe)$, graphite (C), and water (H_2O) nanofluid flow with heat transfer by radiation and convection is explained through graphs (3-45), by observing the various characteristics parameters such as, Weissenberg number parameter (We), Magnetic body force parameter(M), convective energy parameter (Biot) (Bi), Forchheimer parameter (Λ), radiation parameter (F), non uniform heat source and sink (A, B), Nusselt number (Nu) and Skin friction coefficient (C_f). The present computation takes the following parameter values as $(We = 0.3, M = 1.0,\ Bi = 0.5, \Lambda = 1.0, F = 0.5,\ Da = 0.1,\ A = 0.1,\ B = 0.1)$. The thermophysical characteristics of the materials utilised are given by Table 2.

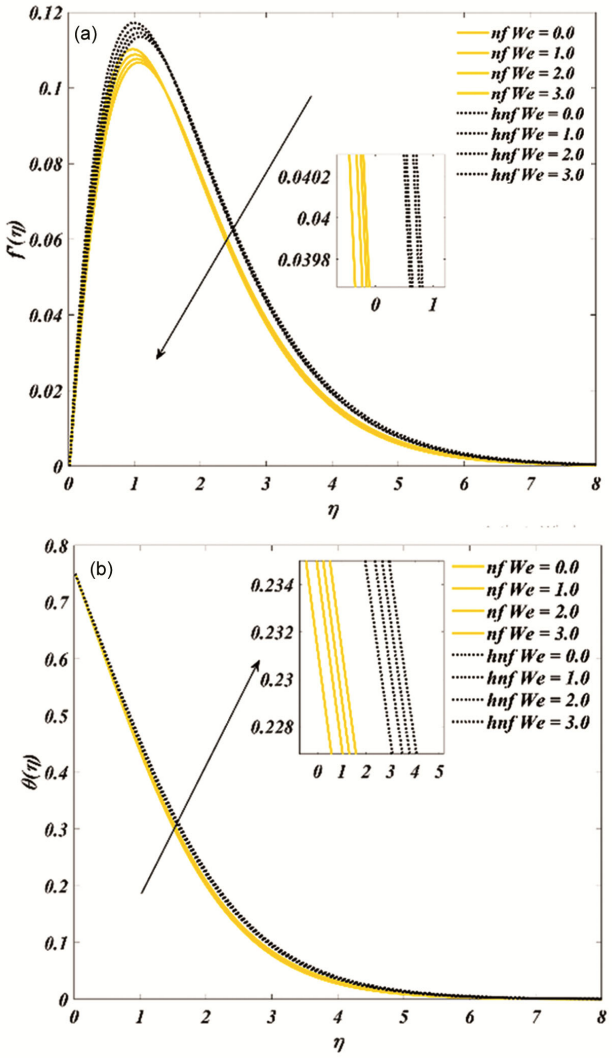

Fig. 3 — (a) Velocity $f'(\eta)$ and (b) temperature $\theta(\eta)$ for different levels of the Williamson fluid parameter (We)

Fig. 3(a) depicts the velocity profile for various values of the Weissenberg number(We), which indicates a diminishing trend in the momentum of the boundary layer as (We) increases$(0 \leq We \leq 3.0)$. (We) arises only in the momentum as a mixed derivative $(We\, f''\, f''')$. Weissenberg number (We) measures the relative effects of viscosity to elasticity. Weissenberg number of zero corresponds to a purely Newtonian fluid, and infinite Weissenberg number corresponds to a purely elastic solid. The fixed values of flow parameters are $Pr = 7.0,\ A = 0.1,\ B = 0.1,\ F = 0.5,\ M = 1.0,\ Bi = 0.5,\ Da = 0.1)$. This phenomenon might be explained by a higher barrier to the movement of Williamson fluid. Fig. 3(b) shows the temperature field of the Williamson fluid for several physical characteristic impacts. The rise in

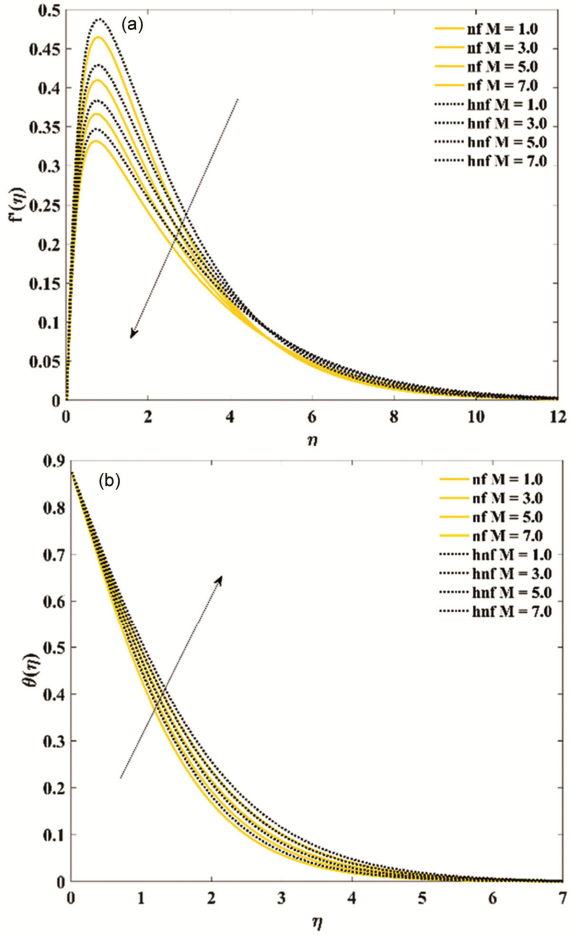

Fig. 4 — (a) Velocity $f'(\eta)$ and (b) temperature $\theta(\eta)$ for different levels of the parameter (M)

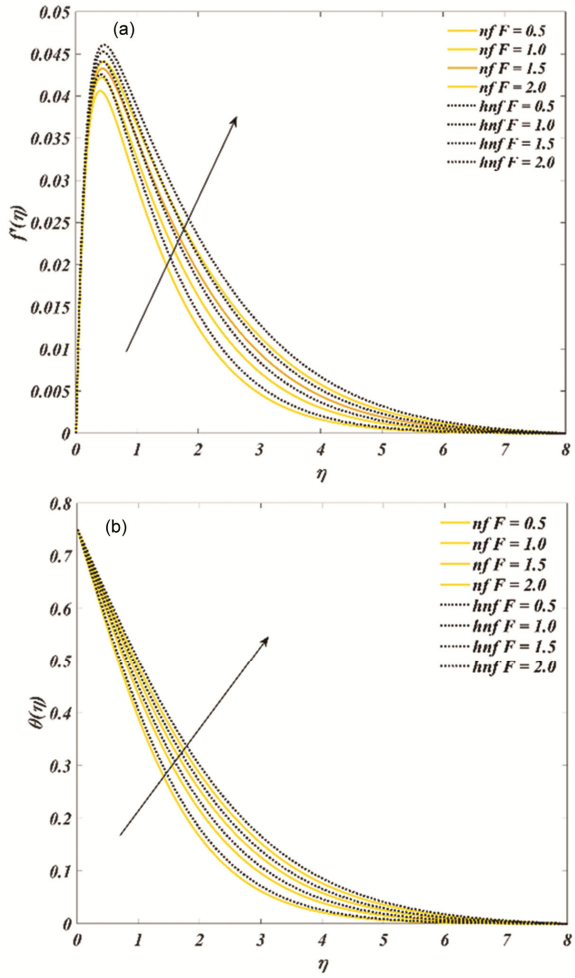

Fig. 5 — (a) Velocity $f'(\eta)$ and (b) temperature $\theta(\eta)$ for different levels of the parameter (F)

(We) causes a growing pattern in the energy boundary layer too. Both the velocity (f') and temperature (θ) results for hybrid nano fluid are the high influence comparing to the nanofluid.

Fig. 4(a) depicts the influence of various magnetic body force parameters $(1.0 \leq M \leq 7.0)$ on velocity profiles when the other values remained constant. It can be observed that as M increases, the velocity distribution decreases.This trend might be ascribed to magnified Lorentz force, in which the rising influence of magnetic body force parameters (M) opposes the movement of the Williamson fluid, resulting in a drop in velocity profile. Fig. 4(b) shows that the temperature is strongly enhanced with greater magnetic field. This magnetic force energizes the boundary layer and increases thermal boundary layer thickness.

Figs 5 (a) and (b) illustrate the velocity and temperature profiles for various values of the heat radiation variable $(0.5 \leq F \leq 2.0)$, respectively. The level of velocity and temperature in the Williamson fluid is supposed to be much greater depending on the radiation parameters. The radiation parameter represents the relative importance of radiant heat transmission over the conductive heat transfer. Thermal radiation now increases the thermal dispersion of the nanoflow. Enhancing the thermal radiation parameter, heat will be introduced to the system and thereby boundary layer thickness of both the flow velocity and energy will increase.

Fig. 6 shows that increasing the Darcy parameter (Da) escalates the velocity (Fig. 6a) and diminishes the temperature (Fig. 6b) considerably. The Darcian parameter, also known as Darcy permeability, is a measure of the ability of a porous medium to allow fluid flow through it. In velocity Eq. (10), the Darcian

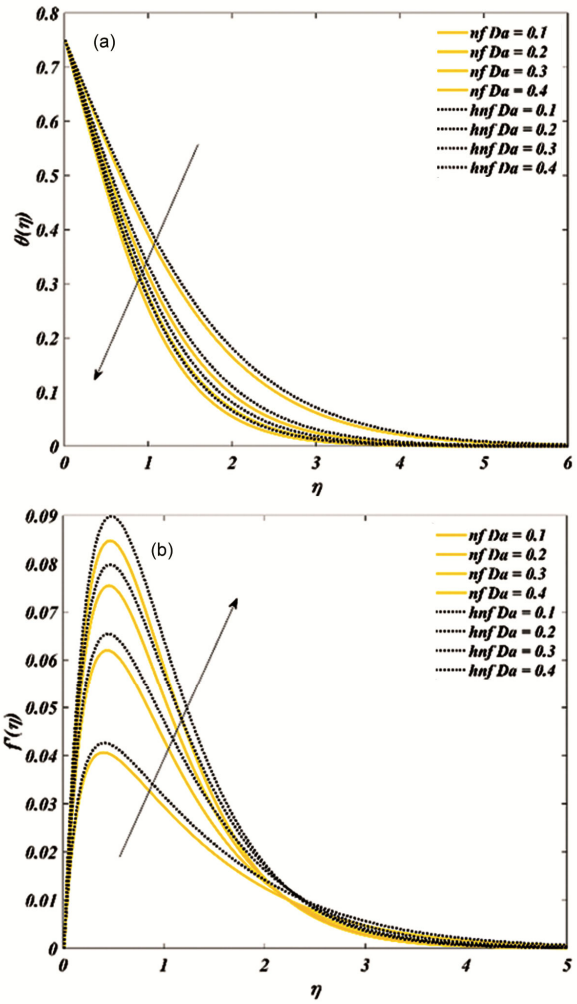

Fig. 6 — (a) Velocity $f'(\eta)$ and (b) temperature $\theta(\eta)$ for different levels of the parameter (Da)

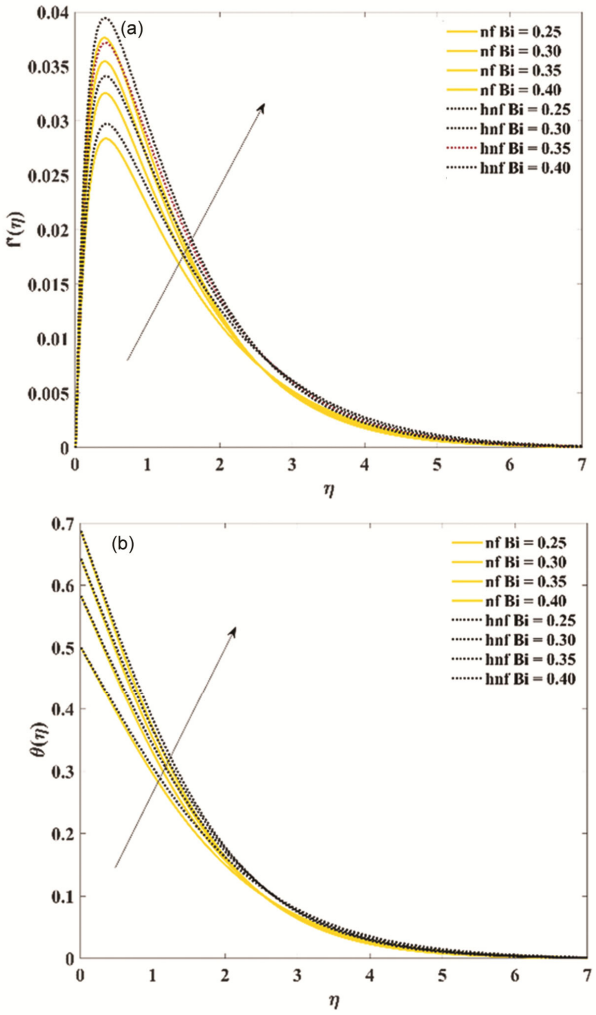

Fig. 7 — (a) Velocity $f'(\eta)$ and (b) temperature $\theta(\eta)$ for different levels of the parameter (Bi)

force $\frac{-f'}{Da}$ also known as a drag force.The accessible surface space for convection heat transmission is reduced, thereby cooling the regime. The result is velocity (f') increases and temperature decreases.

Figs 7 (a) and (b) show the effect of the Biot number (Bi) on the velocity $(f'(\eta))$ and temperature $(\theta(\eta))$ of hybrid-class nanofluid *CdTe* & *C/H₂O*, respectively. Biot number, a measure of the proportion of temperature resistance within the body and at the outermost layer of the body, is utilised in heat transfer estimates. The value of Biot number $(0.25 \leq Bi \leq 0.4)$ and other parameter values are $(Pr = 7.0, A = 0.1,\ B = 0.1,\ F = 0.5,\ M = 1.0,\ We = 0.2,\ Da = 0.1)$. Increasing Biot number, increases the thermal variation and momentum of the nanoflow, owing to the homogenous temperature gradients throughout the body. Situations with a very small Biot number are easier to analyse as the thermal effects *Bi* values in this case are limited to 0.25 to 0.4 (small values). Because of the nonuniformity of the thermal fields inside the flow system, increasing Biot number increases both the flow momentum and energy.

Figs 8 (a) and (b) depict the fluctuation of the velocity and temperature fields with varying transversal dimensions (ξ), respectively. The momentum at the cylinder surface is found to be maximum closer to the lowest stagnation point and decreasing with growing distance beyond it. With progressive distance along the cylinder surface from the lower stagnation point $(\xi = 0)$, as shown in Fig. 8(a) momentum boundary layer thickness is therefore increased marginally with (ξ) values.

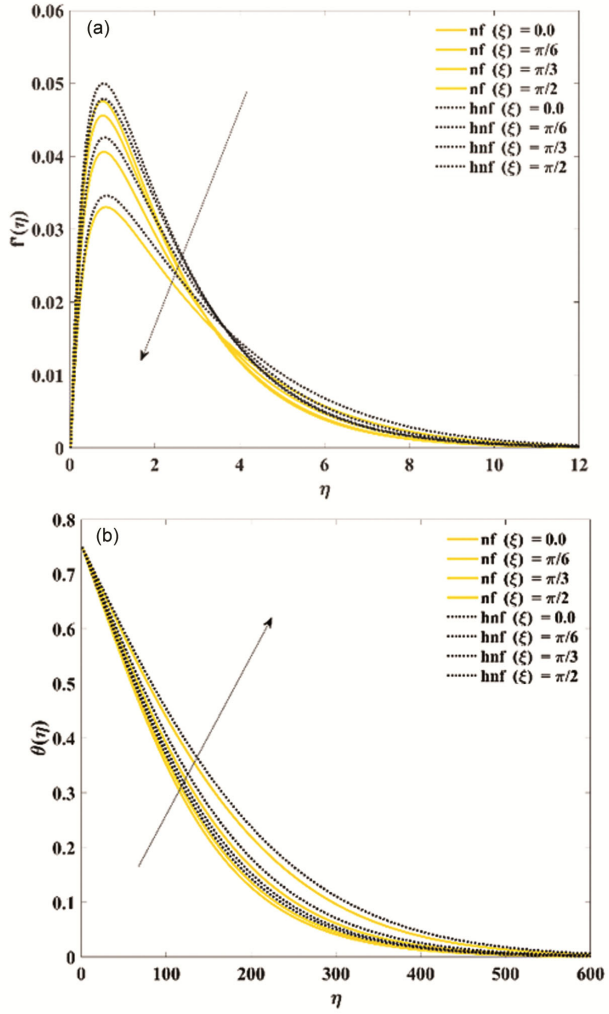

Fig. 8 — (a) Velocity $f'(\eta)$ and (b) temperature $\theta(\eta)$ for different levels of the parameter (ξ)

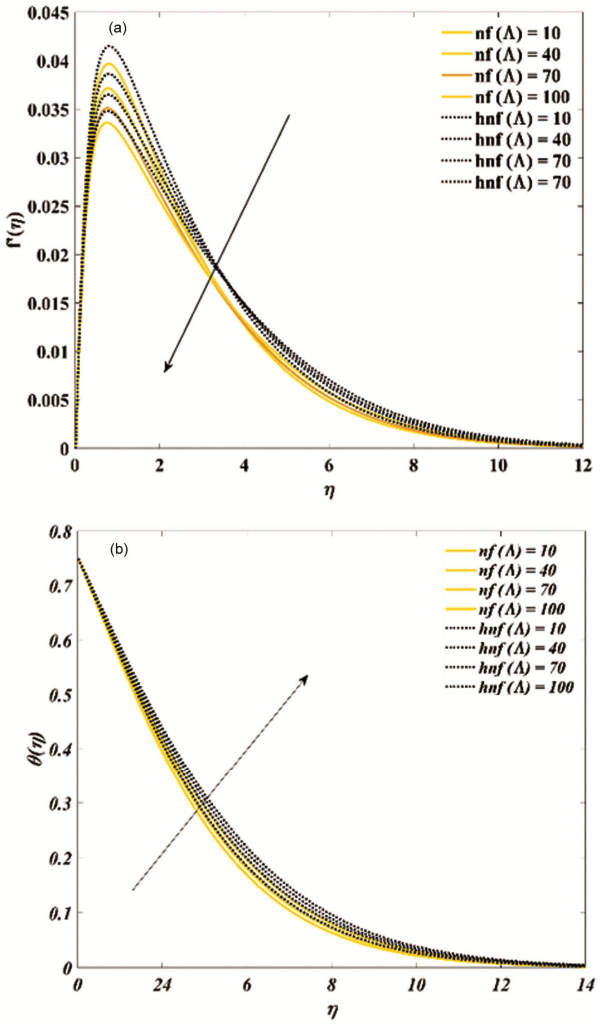

Fig. 9 — (a) Velocity $f'(\eta)$ and (b) temperature $\theta(\eta)$ for different levels of the parameter (Λ)

Conversely a weak enhancement in temperature is observed in Fig. 8(b) with increasing (ξ) values. Consequently, the temperature at the outer edge of the boundary layer also increases significantly with increasing ξ. In simpler terms, as we move further around the cylinder, the temperature at the edge of the hot zone gets hotter (Fig. 8b).

Figs 9 (a), and (b) demonstrate that the Forchheimer inertial factor (Λ) affects the flow parameters. The value of this parameter is linked to the Forchheimer resistant term of second order, $\xi\,\Lambda(f')^2$ in momentum Eq. (10). Forchheimer drag is directly proportional to parameter Λ. As seen in Fig. 9(a), increasing Λ, slows the flow. The impact of Forchheimer drag on velocity is most pronounced within the boundary layer. This is a thin region near the solid surface of the porous medium where the fluid velocity slows down due to friction. The values of Forchheimer inertial parameter $(5 \le \Lambda \le 50)$ increasing the Forchheimer inertial factor (Λ) values, decreases the velocity $\left(f'(\eta)\right)$ whereas temperature $\theta(\eta)$ is increasing.

Fig. 10 show the increasing values of irregular heat source constants (A, B) on $\theta(\eta)$. For irregular heat source characteristics, the internal temperature of the nanoparticles rises the values of A $(0 \le A \le 0.3)$ and values of B $(0 \le B \le 0.3)$. Enhancing A and B values rises the temperature $\theta(\eta)$. Figs 11 to 15 show the Skin friction coefficient (Cf) and Nusselt number (Nu) for the parameters (We, M, Da, Bi, Λ).

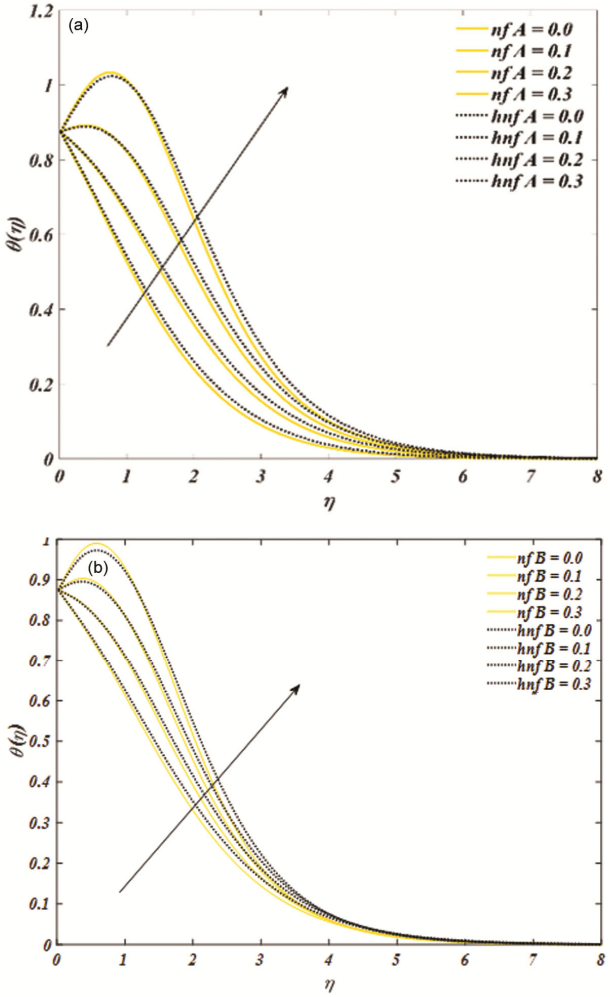

Fig. 10 — Temperature $\theta(\eta)$ for different levels of the heat source constants (a) A and (b) B

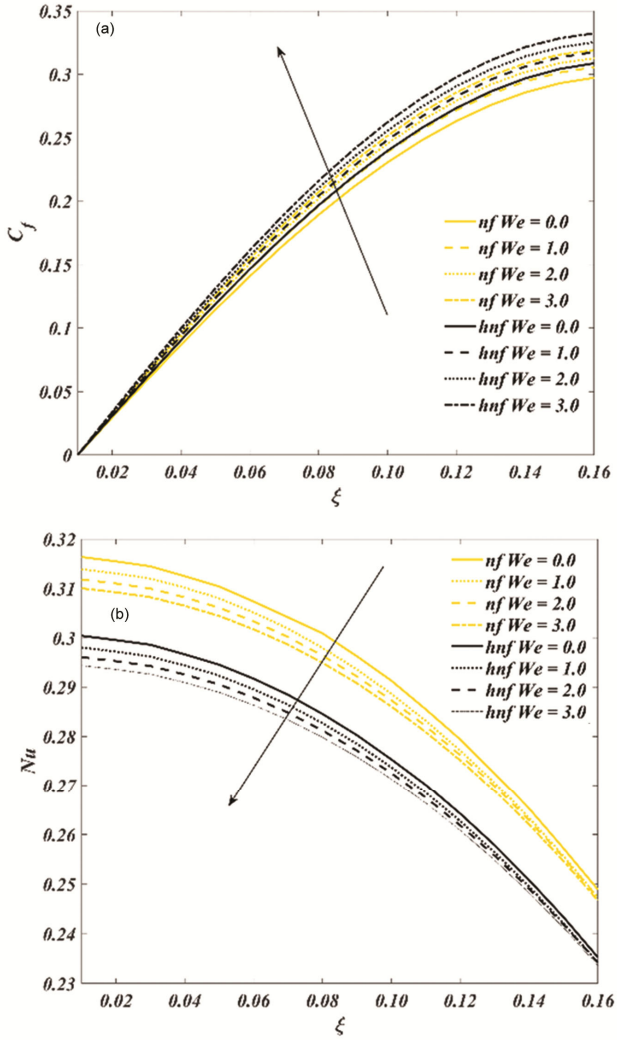

Fig. 11 — Illustration of (a) (C_f) and (b) (Nu) for varied (We)

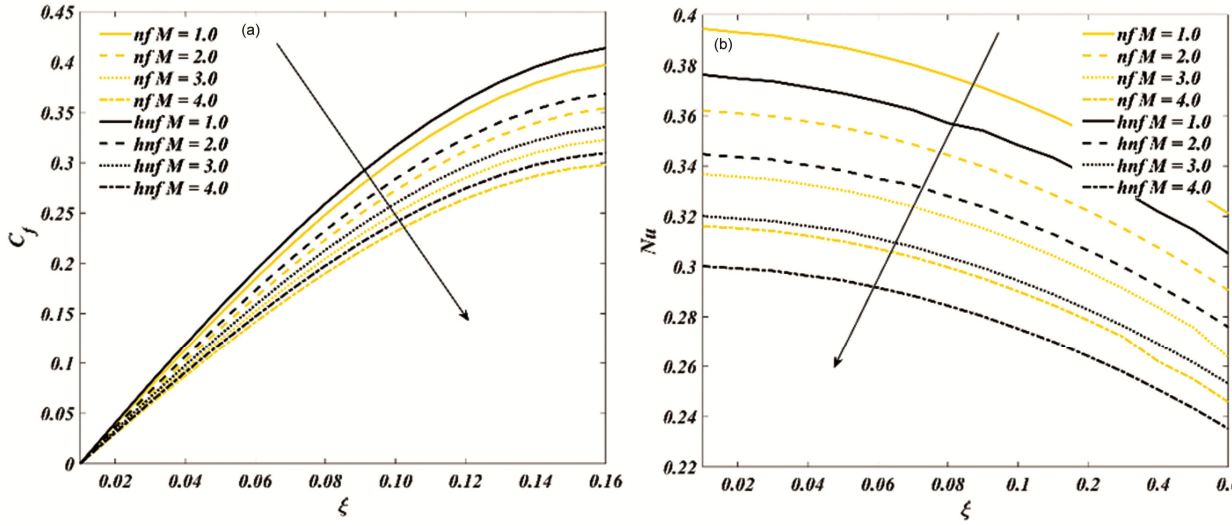

Fig. 12 — Illustration of (a) (C_f) and (b) (Nu) for varied (M)

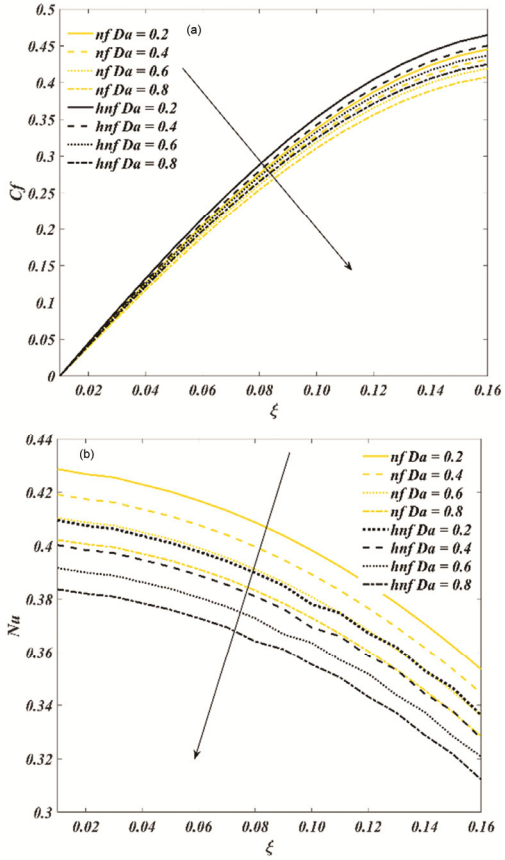

Fig. 13 — Illustration of (a) (C_f) and (b) (Nu) for varied (Da)

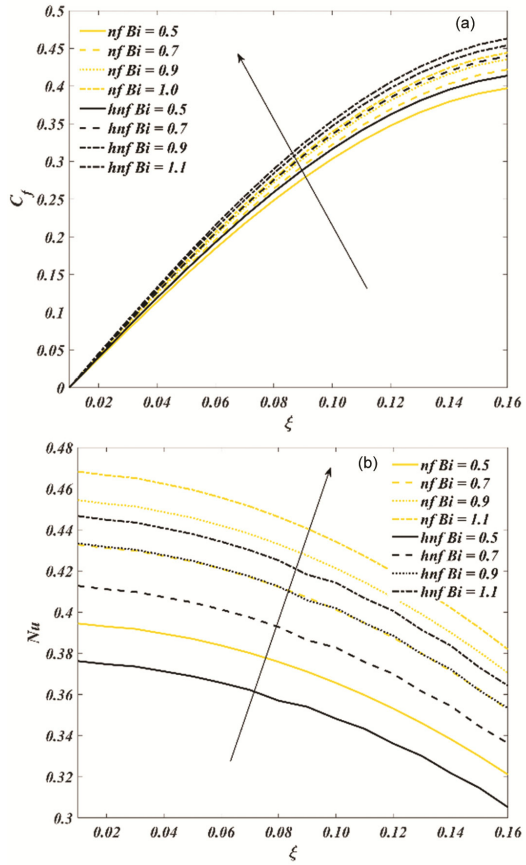

Fig. 14 — Illustration of (a) (C_f) and (b) (Nu) for varied (Bi)

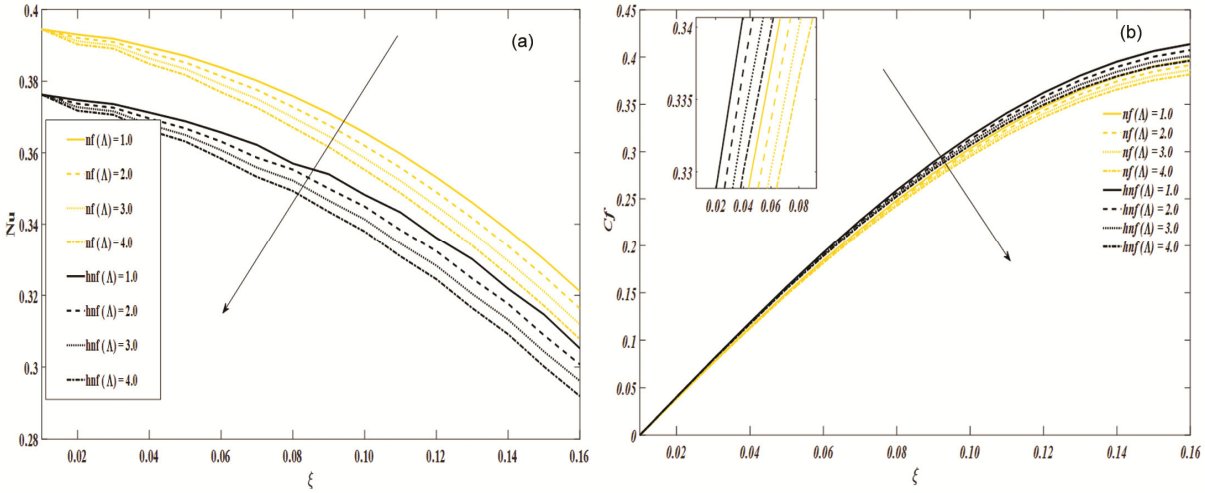

Fig. 15 — Illustration of (a) (Nu) and (b) (C_f) for varied (Λ)

Figs S1–S6 (in Supplementary Information) show the distribution of streamlines ψ. The flow pattern of the streamlines (ψ) with (M), (Da) and (We) is shown in the figures. From the figures, minimal velocity is found in the absence of (Ca) *and* (ψ) (no convective heat transfer), but the amount of energy flow is uniform in all the levels. The $M = 1.0,\ 2.0$ values of the nano fluid, hybrid nanofluid mixture and hybrids nanofluid graphs are shown in Figs S1 and S2. The streamlines for

different Darcy number are drawn for the nanofluid combinations, and hybrid nanofluid (Figs S3 and S4), and the $We = 1.0,2.0$ values of the nanofluid, hybrid nanofluid mixture and hybrids nanofluid graphs shows in Figs S5 and S6.

Conclusion

The heat transfer properties and flow behaviour of a hybrid nanofluid ($CdTe\ and\ C\ /\ H_2O$) passing a horizontal circular cylinder are studied. Using appropriate similarity transformations, the governing equations are changed from higher order PDE to first order PDE. The resultant system of differential equations is solved using the (KBM) technique, and the output are graphed. This work may be expanded to investigate the behaviour of other non-Newtonian fluids under various physical conditions by examining the suspension of several classes of nanoparticles that are appropriate for the real scenario. Heat transfer properties are higher in nanoflows than hybrid nanoflows. Hybrid nanoflow enhances the temperature more than nanofluids. Nanoflow energy enhances for augmenting non-uniform energy source, Forchheimer number and Biot number but opposite behaviour is observed for incrementing Darcy number. Hybrid nanofluids have higher skin friction coefficient than nanofluids.

Supplementary Information

Supplementary information is available on the website http://nopr.niscpr.res.in/handle/123456789.

Symbols are listed as follows

a Cylindrical radius (m)

B_0 Radial magnetic field

x Stream wise coordinate (m)

C_f Skin friction coefficient

y Transverse coordinate (m)

Gr Grashof number

We Weissenberg (viscoelasticity)number

g Acceleration due to gravity $\left({}^{m}/_{s^2}\right)$

u, v Nondimensional velocity elements in the x- and y-axes

k Thermal conductivity of fluid $\left(\frac{W}{m}K\right)$

T Temperature (C)

Nu Local Nusselt number

Pr Prandtl number

c_p At steady pressure, specific heat ($\frac{kJ}{kg}$ ℃)

M Magnetic body force parameter

$A\ and\ B$ Non uniform heat source and sink

F Radiation parameter

Bi A Newtonian heating variable that is non-dimensional

Greek symbols

α Thermal diffusivity (m^2/s)

ν Kinematics viscosity $({}^{m^2}/_{s})$

β Coefficient of thermal expansion $(℃^{-1})$

Γ Time dependent constant

θ Non-dimensional temperature

σ Fluid with high electrical conductivity

η Dimensionless transverse coordinate

ρ Density of viscoelastic fluid (kgm^{-3})

ξ Dimensionless steam wise coordinate

ψ Dimensionless steam wise coordinate

Subscripts

w The state of the wall

∞ Free-flowing circumstances

References

1 Ahmad I, Zan-Ul-Abadin Q, Faisal M, Loganathan K, Javed T & Namgyel N, Convective heat transport in bidirectional water driven hybrid nanofluid using blade shaped cadmium telluride and graphite nanoparticles under electro magnetohydrodynamics process, *J Mathemat*, 2022 (2022) 4471450.

2 Sheikh N A, Ching D L, Khan I, Sakidin H B, Jamil M, Khalid H U & Ahmed N, Fractional model for MHD flow of Casson fluid with cadmium telluride nanoparticles using the generalized Fourier's law, *Sci Rep*, 11 (2021) 16117.

3 Shahzad F, Jamshed W, Safdar R, Rehman Z & Din S M, Heat transfer enhancement in stagnation point flow of nanofluid towards a linear stretching sheet with induced magnetic field: A Keller box strategy, *J Appl Math Mech*, (2022) e202200100.

4 Sreenivasulu P, Poornima T, Reddy N B & Reddy M G, A numerical analysis on UCM dissipated nanofluid imbedded carbon nanotubes influenced by inclined Lorentzian force along with non-uniform heat source/sink, *J Nanofluids*, 8 (2019) 1076.

5 Sreenivasulu P, Reddy N B & Poornima T, Variable thermal conductivity influence on hydromagnetic flow past a stretching cylinder in a thermally stratified medium with heat source/sink, *Front Heat Mass Transf*, 9 (2017) 1.

6 Sreenivasulu P, Poornima T & Reddy P B, Soret and dufour effects on MHD non-darcian radiating convective flow of micropolar fluid past an inclined surface with non-uniform surface heat source or s*ink and chemical reac*tion, In *IOP Conf Ser Mater Sci Eng*, 263 (2017) 062014.

7 Konda J R, MReddy N P M, Konijeti R & Dasore A, Effect of non-uniform heat source/sink on MHD boundary layer flow and melting heat transfer of Williamson nanofluid in porous medium, *Multidiscip Model Mater Struct*, 15 (2019) 452.

8 Jyotshna M & Dhanalaxmi V, Impact of activation energy and heat source/sink on 3D flow of Williamson nanofluid with gan nanoparticles over a stretching sheet, *Europ J Mathemat Statist*, 3 (2022) 16.

9 Song Y Q, Hamid A, Sun T C, Khan M I, Qayyum S, Kumar R N, Prasannakumara B C, Khan S U & Chinram R, Unsteady mixed convection flow of magneto-Williamson nanofluid due to stretched cylinder with significant non-uniform heat source/sink features, *Alex Eng J*, 61 (2022) 195.

10 Swain K, Parida S K & Dash G C, Effects of non-uniform heat source/sink and viscous dissipation on MHD boundary layer flow of Williamson nanofluid through porous medium, *Defect and Diffusion Forum*, 389 (2018) 110.

11 Hamdan M H, Silva-Zea R, Erazo-Bone R, Chuchuca-Aguilar F & Escobar-Segovia K, Plane transverse MHD flow through porous media, *J Appl Mathemat Phys*, 8 (2020) 2115.

12 Geindreau C & Auriault J L, Magnetohydrodynamic flows in porous media, *J Fluid Mech*, 466 (2002) 343.

13 Acharya A K, Dash G C & Mishra S R, Free convective fluctuating MHD flow through porous media past a vertical porous plate with variable temperature and heat source, *Phys Res Int*, 2014 (2014) 587367.

14 Krishna M V, Jyothi K & Chamkha A J, Heat and mass transfer on MHD flow of second-grade fluid through porous medium over a semi-infinite vertical stretching sheet, J *Porous Media*, 23 (2020) 751.

15 Raghunath K, Obulesu M & Sivaprasad R, Heat and mass transfer on an unsteady MHD flow through porous medium between two porous vertical plates, *AIP Conf Proc* 2220 (2020) 130003.

16 Mishra S R, Hoque M M, Mohanty B & Anika N N, Heat transfer effect on MHD flow of a micropolar fluid through porous medium with uniform heat source and radiation, *Nonlinear Eng*, 8 (2019) 65.

17 Naqvi S M, Waqas H, Yasmin S, Liu D, Muhammad T, Eldin S M & Khan S A, Numerical simulations of hybrid nanofluid flow with thermal radiation and entropy generation effects, *Case Stud Therm Eng*, 40 (2022) 102479.

18 Raza A, Thumma T, Khan S U, Boujelbene M, Boudjemline A, Chaudhry I A & Elbadawi I, Thermal mechanism of carbon nanotubes with Newtonian heating and slip effects: A prabhakar fractional model, *J Indian Chem Soc*, 99 (2022) 100731.

19 Ahmad I, Zan-Ul-Abadin Q, Faisal M, Loganathan K, Javed T & Chaudhary D K, Prescribed thermal activity in the radiative bidirectional flow of magnetized hybrid nanofluid: Keller-box approach, *J Nanomater*, 27 (2022) 2022.

20 Sheikh N A, Ching D L, Khan I & Sakidin H, Intensification in heat transfer due to hybrid nanoparticles embedded in sodium alginate, *Case Stud Therm Eng*, 28 (2021) 101440.

21 Ghani S N, Ul-Haq R & Noor N F, Engine oil enhanced performance with hybrid graphene-SWCNT nanomaterials over a Riga curvy surface, *Case Stud Therm Eng*, 45 (2023) 102902.

22 Waqas H, Farooq U, Liu D, Abid M, Imran M & Muhammad T, Heat transfer analysis of hybrid nanofluid flow with thermal radiation through a stretching sheet: A comparative study, *Int Commun Heat Mass Transf*, 138 (2022) 106303.

23 Song H C, Xie C Y, Kong Q, Wei L & Wang X T, Daylight ultraviolet B radiation ruptured the cell membrane, promoted nucleotide metabolism, and inhibited energy metabolism in the plasma of pacific oyster, *Sci Total Environ*, 862 (2023) 160729.

24 Khan W A, Waqas M, Chammam W, Asghar Z, Nisar U A & Abbas S Z, Evaluating the characteristics of magnetic dipole for shear-thinning Williamson nanofluid with thermal radiation, *Comput Methods Prog Biomed*, 191 (2020) 105396.

25 Mishra S, Mondal H & Kundu P K, Analysis of Williamson fluid of hydromagnetic nanofluid flow in the presence of viscous dissipation over a stretching surface under radiative heat flux, *Int J Appl Comput Mathemat*, 9 (2023) 58.

26 Rao A S, Prasad V R, Beg O A & Rashidi M, Free convection heat and mass transfer of a nanofluid past a horizontal cylinder embedded in a Non-darcy porous medium, *J Porous Media*, 21 (2018) 1.

27 Cebeci T & Bradshaw P, Physical and computational aspects of convective heat transfer, Springer Science & Business Media, *Springer,* New York, (2012).

28 Subba R A, Amanulla C H, Nagendra N, Anwar B O & Kadir A, Hydromagnetic flow and heat transfer in a Williamson Non-newtonian fluid from a horizontal circular cylinder with newtonian heating, *Int J Appl Comput Mathemat*, 3 (2017) 3389.

29 Nazar R, Amin N S & Pop I, Free convection boundary layer on an isothermal horizontal circular cylinder in a micropolar fluid, *Int Heat Transfer Conf Digit Lib*, (2002).

30 Subba R A, Amanulla C H, Nagendra N, Anwar B O & Kadir A, Hydromagnetic flow and heat transfer in a Williamson Non-newtonian fluid from a horizontal circular cylinder with newtonian heating, *Int J Appl Comput Mathemat*, 3 (2017) 3389.

31 Keller H B & Cebeci T, Accurate numerical methods for boundary layer flows 1. Two dimensional flows, *Proc Int Conf Numer Meth Fluid Dyn*, Springer, New York (1971).